Influence of a Lanthanide Ion on the Ni Site of a Heterobimetallic 3d–4f Mabiq Complex

Stuart Boyce, Jules Moutet, Lukas Niederegger, Thomas Simler, Grégory Nocton, Corinna Hess

Influence of a Lanthanide Ion on the Ni Site of a Heterobimetallic 3d-4f Mabiq Complex

Stuart A. J. Boyce,[a,c] Jules Moutet,[b] Lukas Niederegger,[a] Thomas Simler,[b] Grégory Nocton[b] and Corinna R. Hess*[a]*

[a] Department of Chemistry and Catalysis Research Center (CRC), Technische Universität München, Lichtenbergstraße 4, 85748 Garching, Germany

[b] LCM, CNRS, École Polytechnique, Institut Polytechnique de Paris, Route de Saclay, 91128 Palaiseau Cedex, France

[c] School of Chemistry, The University of Edinburgh, Joseph Black Building, David Brewster Road, Edinburgh, EH9 3FJ, United Kingdom

KEYWORDS Ytterbium, nickel, heterobimetallic complexes, redox-active ligand, macrocyclic ligand

ABSTRACT

This work presents the synthesis and characterization of a 3d-4f bimetallic complex based on the redox-active macrocyclic biquinazoline ligand, Mabiq. The mixed Yb-Ni complex, $[(Cp^*)_2Yb(Mabiq)Ni]BArF$ (**3**), was synthesized upon reaction of $[Ni^{II}(Mabiq)]BArF$ (**2**) with $Cp^*_2Yb^{II}OEt_2$. The molecular structures of **3** and its sister complex, $[(Cp^*)_2Yb(Mabiq)Ni][(Cp^*)_2Yb(OTf)_2]$ (**1**), confirmed the presence of a Yb(III) center and a reduced Ni-Mabiq unit. Spectroscopy (absorption and NMR), cyclic voltammetry and magnetic susceptibility studies were employed to analyze the electronic structure of **3**, which is best described by the $[(Cp^*)_2Yb^{III}(Mabiq^{\bullet})Ni^{II}]^+$ formulation. Notably, the ligand centered radical is delocalized over both the diketiminate and bipyrimidine units of the Mabiq ligand. The magnetic susceptibility and variable temperature NMR studies for **3** denote coupling between the Ni-Mabiq site and the peripheral Yb center – previously unobserved in 3d-3d Mabiq complexes. The complex nature of the exchange interactions is highlighted by the multiconfigurational ground state for **3**, comprising nearly degenerate singlet and triplet states.

INTRODUCTION

The synergistic chemistry that can arise from the combination of d and f-block metals has prompted interest in 3d-4f complexes in particular.[1-4] The predominant research involving these complexes has unarguably been in the fields of molecular magnetism and catalysis.

A surge of activity in the field of single molecule magnets (SMMs) followed the report of the first 3d-4f SMM by Mrozinski and co-workers in 2004.[5-9] The strength of the 3d-4f interactions and the nature of each magnetic center can dramatically influence the SMM properties. Strong interaction between a paramagnetic Ln^{III} ion and another paramagnetic center is an effective way for improving SMM performance, as illustrated by Cr^{III}- and Co^{III}-Dy^{III} systems, which exhibit substantial thermal energy barriers to magnetic reorientation as a consequence of exchange interactions between the two metal centers.[10-12] However, 3d-4f interactions are not always beneficial to SMM performance, as evidenced by McInnes *et al.* through a series of butterfly-like M_2Ln_2 (M = Mg^{II}, Mn^{III}, Co^{II} - Cu^{II}; Ln = Y^{III}, Gd^{III} - Er^{III}) structures, in which even weak exchange interactions resulted in a decreased effective energy barrier.[13] Therefore, a better understanding of the magnetic exchange interactions in 3d-4f compounds is still needed to effectively utilize these systems as SMMs.

Catalysis involving 3d-4f complexes also is a quickly developing field; lanthanides can have a marked effect on both small molecule and organometallic reactions. Domino, Friedel-Crafts, Mannich, Michael addition and cross-coupling reactions have all been successfully catalyzed by polynuclear 3d-4f coordination clusters.[14, 15] Enhanced CO_2 transformations by asymmetric Zn-Ln complexes,[16-19] and catalytic olefin hydrogenation promoted by Ni-Lu complexes—in which lanthanide coordination was crucial for tuning and exploiting the reactivity at the Ni center—have also been reported in the last five years.[20] Lanthanides incorporated into Mn-based water

oxidation cluster mimics modulate the Mn potentials, as well as the O-atom transfer activities of these systems.[21, 22] The first examples of molecular 3d-4f water oxidation catalysts (WOCs), a Co_3Ln (Ln = Ho-Yb) cubane series reported by Evangelisti *et al.*, also showed enhanced photocatalytic performance compared to Co-only molecular WOCs.[23]

Recently, several of these mixed-metal systems have also incorporated redox-active ligands, which offers further potential for both catalysis and magnetism.[24-29] In the field of transition metal chemistry — through their ability to participate in redox transformations — these ligands act as 'electron storage sites', thereby opening up the reactive possibilities of the complex as a whole.[30-33] Ligand-based reactivity has not been robustly developed within lanthanide chemistry. However, investigations into 4f-complexes with e.g. redox-active Schiff bases and aminophenolate ligands have shown how these ligands can support the formation of reduced lanthanide ions.[34-36] Despite the number of reports with either 3d or 4f centers in combination with redox-active ligands, complexes comprising all three groups are surprisingly limited.[37-40] Given the evidence for improved magnetic properties in systems with two paramagnetic centers, synthesizing 3d-4f systems comprising redox-active ligands — in which a ligand radical can exist alongside a paramagnetic lanthanide — offers further opportunities to modulate and exploit exchange interactions. An example is the study by Goudy *et. al.* concerning the $[(Cp^*)_2Yb(L)PdMe_2]$ complexes (L = bipyrimidine (bipym) or 4,5,9,10-tetraazaphenanthrene (taphen)).[41] These complexes undergo oxidative addition, resulting in formation of a stable, isolable Pd^{IV} species. The unique combination of redox-active ligands with divalent lanthanide fragments is thus an effective strategy for accessing and stabilizing high oxidation states in organometallic chemistry. This strategy could also be effectively adopted to obtain species behaving as low-valent transition metal compounds for CO activation.[42]

Prompted by the studies with the abovementioned Yb-Pd complexes, and our interest in further developing the chemistry of 3d-4f complexes, we have now focused on the merger of lanthanides with transition metal complexes based on the macrocyclic biquinazoline ligand, Mabiq. Monometallic M-Mabiq complexes exhibit properties that could be further exploited in 3d-4f chemistry; including the electro- and photocatalytic behavior of the Co-Mabiq and Ni-Mabiq systems, respectively.[43, 44] These properties and the unique electronic structures associated with the complexes can in part be accounted for by the established redox-activity of the Mabiq ligand.[45] Several homobimetallic transition metal Mabiq complexes were previously synthesized, and we envisioned that the peripheral bipym unit of the Mabiq ligand would also readily coordinate a lanthanide ion.[46, 47] Similar to the Pd compounds above, the incorporation of a lanthanide could alter the redox and electronic properties of the metal in the central Mabiq cavity, and potentially foster new reactivities by the combined system. The synthesis and characterization of the first 3d-4f Mabiq system, a Yb-Ni complex, are reported herein. This complex provides important insight into the effect of the 4f metal on the M-Mabiq properties and on the metal-metal interactions, that contrasts with properties of the 3d-3d bimetallic Mabiq complexes previously reported.

RESULTS AND DISCUSSION

Synthesis and Solid-State Characterization. The initial attempts to synthesize a heterobimetallic Yb–Ni complex involved the stoichiometric reaction of [Ni(Mabiq)]OTf with ytterbocene, $(Cp^*)_2YbOEt_2$. Whilst this initial synthesis was successful in producing a bimetallic complex, $[(Cp^*)_2Yb(Mabiq)Ni][(Cp^*)_2Yb(OTf)_2]$ **(1)**, the Yb-containing counterion complicates characterization. Similar counterion generation upon production of complexes with the Cp^*_2Yb

fragment in the presence of coordinating triflates was previously observed.[48] Consequently, the diamagnetic tetrakis[3,5-bis(trifluoromethyl)phenyl]borate, (BArF) analogue of [Ni(Mabiq)]OTf, [Ni(Mabiq)]BArF (**2**), was prepared by complexation of the ligand with $NiCl_2 \cdot 6H_2O$ in ethanol and subsequent salt metathesis with NaBArF (Scheme S1). The electronic spectrum and solid state structure of **2** are consistent with those of the previously reported Ni^{II}-Mabiq complex (Figures 2 and S2, Tables S1 and S3).[44] The reaction of **2** with $(Cp^*)_2YbOEt_2$ in cold THF gave the paramagnetic bimetallic [$(Cp^*)_2$Yb(Mabiq)Ni]BArF (**3**) in 78% yield (Scheme 1).

Scheme 1. Reaction of **2** with $(Cp^*)_2YbOEt_2$ in THF (−35 °C) yields the bimetallic **3**.

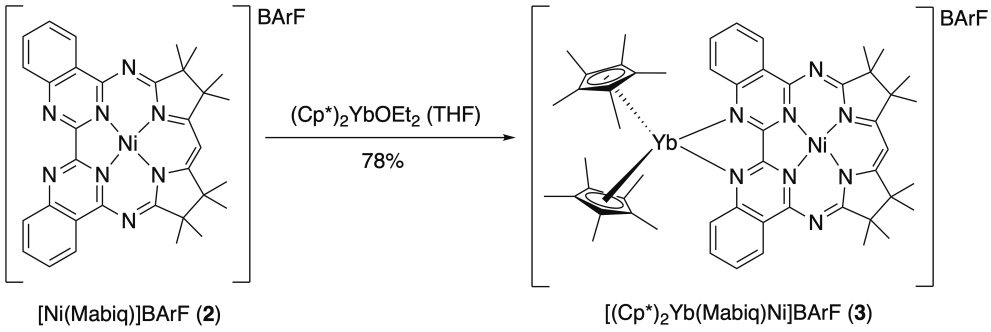

[Ni(Mabiq)]BArF (**2**) [(Cp*)$_2$Yb(Mabiq)Ni]BArF (**3**)

Single crystals of both bimetallic complexes were obtained. However, detailed analysis of the molecular structure of **3** was not possible due to structural disorder, which could not be resolved. The molecular structures, of complex [$(Cp^*)_2$Yb(Mabiq)Ni] in **1** and **3**, exhibit the same connectivity and overall geometry, including a square planar Ni-Mabiq center adjacent to a pseudo-tetrahedral Yb that resides in the peripheral Mabiq coordination site. However, conclusions based on the bond distances, as detailed below, relied on the structure of **1**. The structural similarities of the shared [$(Cp^*)_2$Yb(Mabiq)Ni] component in both **1** and **3** indicate that conclusions concerning the electronic structure of this unit, as deduced from the crystallographic data for **1,** also apply to **3**. All subsequent analyses of the bimetallic complex

(*e.g.* electrochemical, spectroscopic and magnetitic susceptibility studies) were carried out using **3**.

Select bond distances and angles of **1** (Figure 1) are provided in Table 1. The average Yb-Cp* distance (2.315 Å) is consistent with literature values for Yb^{III} centers in Cp compounds.[49] The reported values range from 2.30 – 2.31 Å for Yb^{III} complexes, whilst Cp-Yb^{II} bond distances lie in the range of 2.43 – 2.50 Å. The data clearly denote that oxidation of the lanthanide ion occurred in the reaction of [Ni(Mabiq)]OTf and $(Cp^*)_2Yb(OEt_2)$. The average Ni–N bond distance in **1** (1.877(8) Å) is analogous to that in **2** (1.867(3) Å), which indicates that the Ni ion, on the other hand, remains divalent. Therefore, the corresponding reduction of the Ni-Mabiq site occurs at the ligand. A notable feature of the bimetallic compound is the strongly shortened C1–C33 distance of the bipym (1.40(1) in **1** vs. 1.476(5) Å in **2**), with a corresponding lengthening of the adjacent C-N bonds (1.41(1) and 1.35(1) in **1** vs. 1.374(4) and 1.291(4) in **2**), in support of ligand-centered reduction. Interestingly, the electron density in all previously characterized $[M^{II}(Mabiq^{\bullet})]$ complexes — including in the bimetallic $[Cu^{II}_2(Mabiq^{\bullet})(PPh_3)_2]PF_6$ — is predominantly localized on the diketimine site of the macrocycle; changes in the bond distances of the bipym group were not observed.[43-47] However, the diketiminate bond distances within **1** are similar to those of the ligand in other divalent M^{II}-Mabiq complexes (Table S2).[43] The structural data for **1**, and by extension **3**, supports the $[Yb^{III}(Mabiq^{\bullet})Ni^{II}]^+$ formulation of the bimetallic Yb-Ni compounds. However, the additional variations in the bipym bond lengths in comparison to the monometallic $[Ni^{II}(Mabiq^{\bullet})]$ system, already suggest an altered electronic structure due to the presence of the 4f ion.

Table 1. Select bond distances and angles of **1** compared with previously reported compounds of similar structure.

Atoms	Length / Å or Angle /°	Comparative Literature Values
Yb1 – C(Cp*)	Av. 2.61(2)	Cp^*_2Yb(4,5-diazafluorenyl): Av. 2.609(9) [49]
Yb1 – Ct1,2†	Av. 2.315	Cp^*_2Yb(4,5-diazafluorenyl): Av. 2.31 [49]
Yb1 – N2,8	Av. 2.356(8)	Cp^*_2Yb(4,5-diazafluorenyl): Av. 2.372(1) [49]
Ct1 – Yb1 – Ct2	136.14	Cp^*_2Yb(4,5-diazafluorenyl): 140.00 49
Ni – N	Av. 1.887(8)	$[Ni^{II}(Mabiq^{\bullet})]$: Av. 1.874(15) [44]
C1-C33	1.40(1)	**2:** 1.476(5)

† Ct1,2 denote the calculated centroids of the Cp* rings.

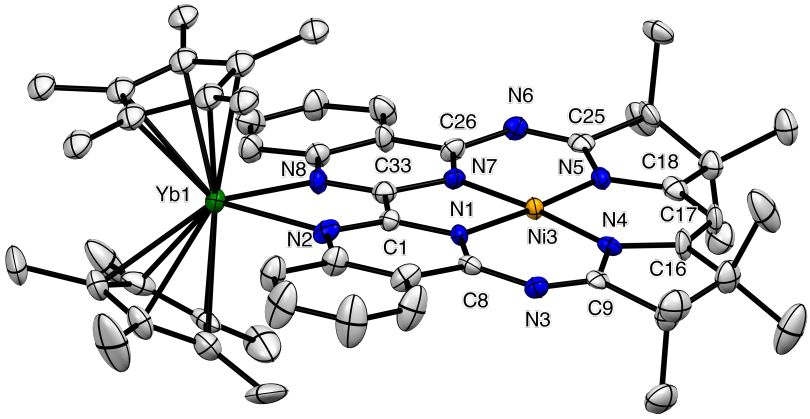

Figure 1. ORTEP structure of **1** with ellipsoids at 50% probability and relevant atoms labelled. Counterion, solvent molecules and H-atoms have been omitted for clarity. Full crystallographic data for both **1** and **3** can be found in Figures S1 and S3 and Tables S1-S2.

Solution State Characterization. Absorption spectroscopy provided further insight into the electronic structure of **3**. The electronic spectrum of the complex in THF exhibits a series of distinctive absorption bands in the visible region (λ_{max}= 794, 708 nm; ε = 0.29, 0.18 × 10^4 M^{-1} cm^{-1}; Figure 2) that are typical of complexes containing the reduced Mabiq ligand.[43-47] These low energy transitions are only slightly shifted with respect to their position in the spectrum of

[Ni^{II}(Mabiq$^{\bullet}$)].[44] Coordination of the Yb has a more significant impact on the transitions in the 400-500 nm region. The spectrum further evidences the presence of a one-electron reduced Mabiq unit in **3**. In contrast to the crystallographic data, however, the data suggests a similar electronic structure as for [Ni^{II}(Mabiq$^{\bullet}$)], in which the radical character was predominantly located at the diketiminate unit. Thus, while the spectrum of **3** is consistent with the [$(Cp^*)_2Yb^{III}$(Mabiq$^{\bullet}$)Ni^{II}]BArF formulation, structural and absorption spectroscopic data alone do not allow for precise assignment of the electronic structure.

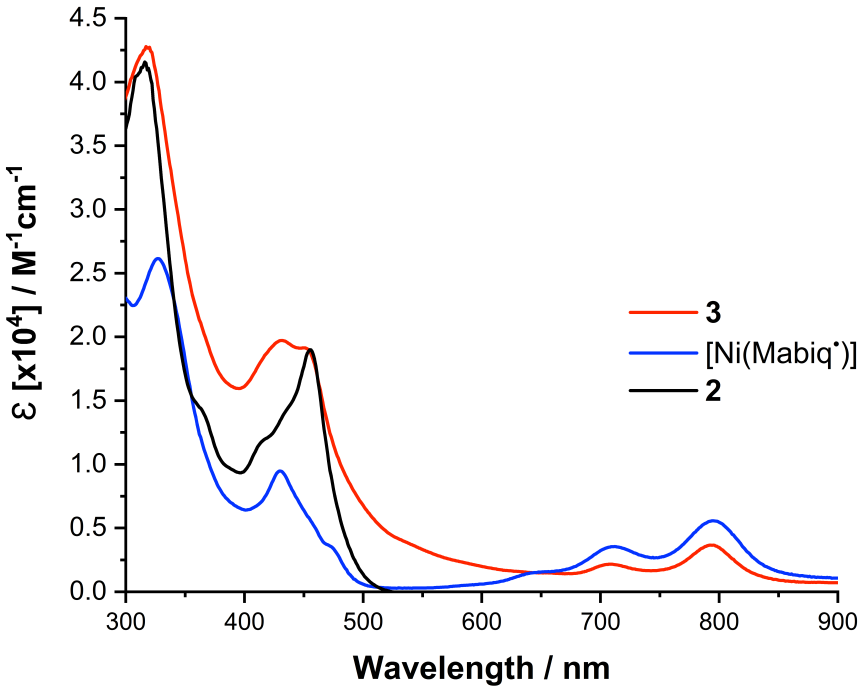

Figure 2. UV-Vis spectra of **2** (black), **3** (red) and [Ni(Mabiq$^{\bullet}$)] (blue).

We subsequently investigated how the presence of the Yb ion affects the redox properties of the Ni-Mabiq unit, since these are particularly relevant for the potential application of these complexes in redox reactions. The cyclic voltammogram (CV) of **3** is shown in Figure 3 (red trace), along with the CV of the monometallic [Ni^{II}(Mabiq$^{\bullet}$)] for comparison (black trace). The latter complex exhibits a reversible $[Ni(Mabiq)]^{+}/[Ni(Mabiq^{\bullet})]^{0}$ couple at −1.04 V vs. $Fc^{+/0}$ (Fc =

ferrocene), as well as additional redox events below –1.90 V, which likely include further reductive processes involving the Mabiq ligand.[44, 46, 47] The CV of **3** also displays a series of reversible couples at −0.71, −1.09 and −1.94 V, and our tentative assignments of these events is as follows. The redox couple at −0.71 V is assigned to the $[Ni(Mabiq)]^{+}/[Ni(Mabiq^{\bullet})]^{0}$ couple, which compared to the CV of $[Ni^{II}(Mabiq^{\bullet})]$, undergoes a notable positive shift (Figure 3). The assignment of this event at −0.71 V is consistent with the observed reduction of $[Ni^{II}(Mabiq)]^{+}$ by $(Cp^{*})_2Yb^{II}$, and the $Yb^{III}/Mabiq^{\bullet}$ formulation of **3**, which signifies that the Ni-Mabiq unit is the more readily reduced species. A positive shift in the M-Mabiq couples was observed upon coordination of a Cu^{I} ion to the outer Mabiq site as well.[47] However, coordination of the trivalent lanthanide to the peripheral binding site appears to have a more dramatic effect on the redox properties of the macrocyclic site, which evidences the stronger electronic influence by the 4f ion. The subsequent events at –1.09 V and –1.94 V, likely include the $Yb^{III/II}$ couple and further reductive events involving the Ni-Mabiq unit. The $Yb^{III/II}$ couple of $Cp^{*}_2Yb(THF)_n$ was reported at −1.48 V vs. $Fc^{+/0}$, and shifted to significantly more negative potentials upon coordination to terpyridine;[50] the $[Ni(Mabiq^{\bullet})]^{0}/[Ni(Mabiq)]^{-}$ couple of the monometallic compound lies at –1.94 V. Therefore, it is difficult to distinguish the two processes.

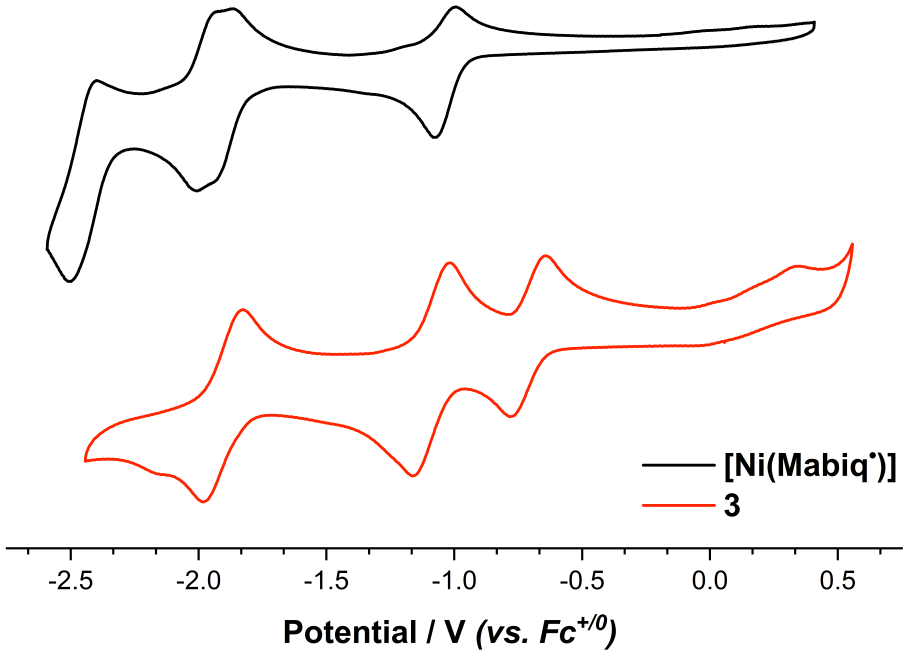

Figure 3. CV of **3** (red; 0.2 V s^{-1}) and [Ni(Mabiq$^{\bullet}$)] (black; 0.1 V s^{-1}); 0.1 M [N(*n*-Bu)$_4$]PF_6, THF.

^{1}H NMR and Magnetic Susceptibility Studies. X-ray and solution state analysis of the redox properties of **3** suggest that the coordination of the lanthanide leads to extended delocalization of spin density in the Mabiq ligand. These studies would be complemented by more detailed analysis of the overall spin density of the complex, as well as of the interaction between the lanthanide fragment and the Ni(Mabiq$^{\bullet}$) fragment. The analysis of the ^{1}H NMR of paramagnetic compounds is useful in this regard, as it relies both on the magnetic susceptibility and on the spin density, while temperature dependent solid-state magnetic data should inform on the nature of the interaction between the multiple spin carriers in the overall molecule.

The ^{1}H-NMR of **2** (Figure S4, $CDCl_3$) shows the expected signals for each of the Mabiq proton environments. A minor downfield shift is only observed for the diketiminate proton resonance, compared to the spectrum of the chloride analogue. All signals are present in the diamagnetic

region and in good agreement with a C_{2v} symmetry in solution. The ^{1}H-NMR of **3** (C_6D_6) at 298 K is distinctly different (Figure 4). The proton resonances of this paramagnetic complex appear across a much larger range from +65 to –10 ppm. In paramagnetic NMR, the observed chemical shift corresponds to the sum of the paramagnetic isotropic shift (δ^{para}) and the diamagnetic shift (δ^{dia}) (Equation 1).[51] The diamagnetic shift can be extracted from the value of the diamagnetic analogue, **2**, which allows calculation of the δ^{para} value. The latter parameter is also composed of two contributions (Equation 2): the pseudo-contact contribution (δ^{PC}) and the Fermi contact contribution (δ^{FC}).[52] δ^{PC} is principally due to the distance of the proton from the main paramagnetic center and the angle of the spin with respect to the principal axis of magnetization. In the case of **3**, both contributions must be considered due to the lanthanide contribution to δ^{PC} and the increased δ^{FC} contribution that arises from the radical character on the Mabiq ligand.

$$\delta^{obs} = \delta^{para} + \delta^{dia} \quad (1)$$
$$\delta^{para} = \delta^{PC} + \delta^{FC} \quad (2)$$

We analyzed the NMR spectrum in an effort to deconvolute both effects. The protons of the Cp* rings readily could be assigned to the signal at –0.76 ppm, which integrates to 30 protons. The eight Mabiq bipym protons (D = 63.54, C = 14.53, A = 1.36 and B = –4.65 ppm) were likewise assigned based on their integrations, by comparison to the NMR spectrum of the related $(Cp^*)_2Yb(bipym)NiMe_2$, and from the variable temperature (VT) NMR study (*vide infra*).[42]

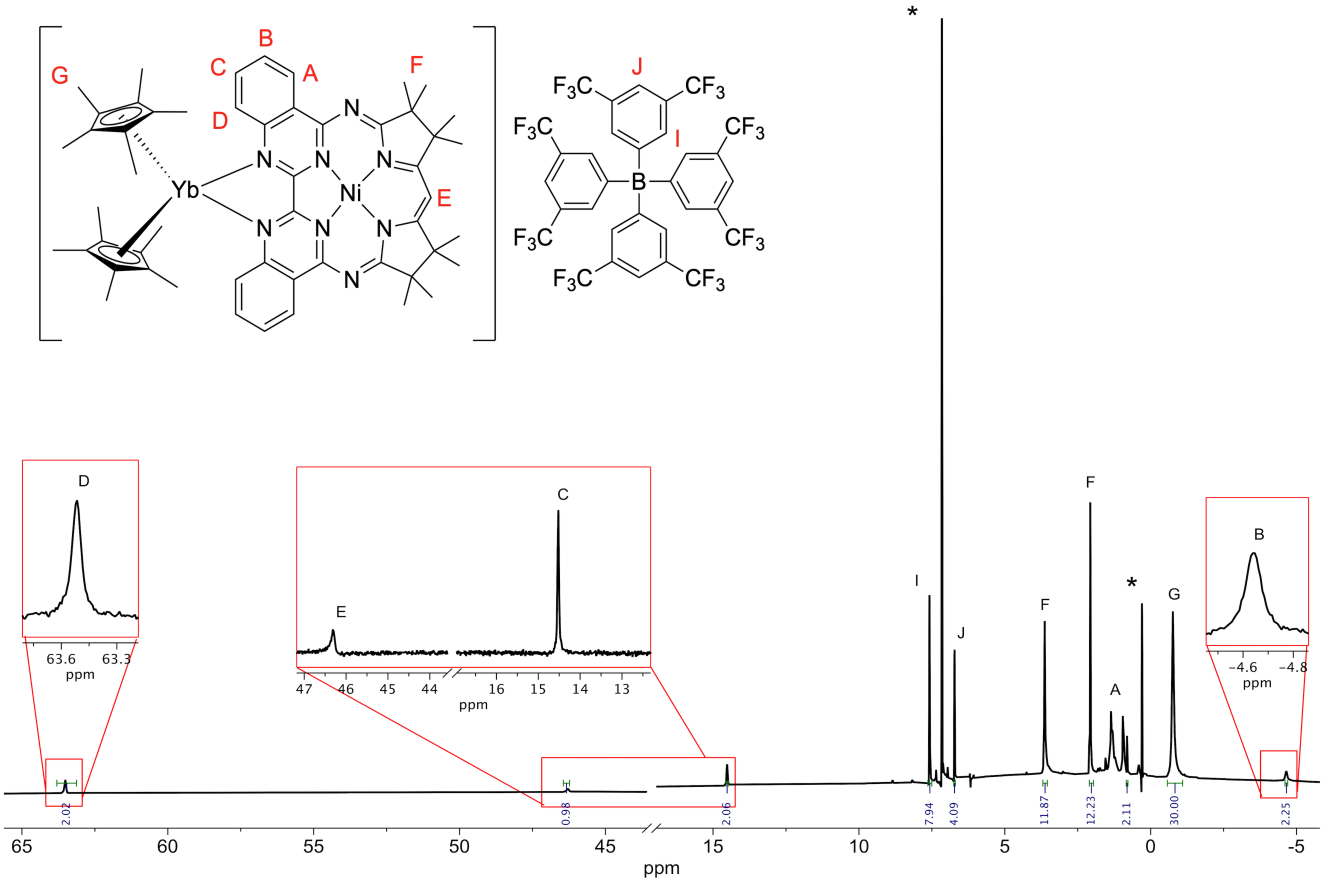

Figure 4. ^{1}H-NMR spectrum of **3** (C_6D_6) and scheme depicting the assignment of the resonances; integrals are normalized relative to the signal for G (30 H).; * indicates residual solvent peaks. Acquisition parameters: spectral width = 500 ppm; number of scans = 512; acquisition time = 0.218 s.

The isotropic paramagnetic chemical shift was calculated for environments A to D and E as –7.19, –12.65, 6.26, 54.37 and 39.76 ppm, respectively (Table S4). The δ^{PC} can be estimated from the distance and angle of each proton from the principal axis of magnetization and is large for both D (3.04 Å, 30°) and C (5.36 Å, 30°); and smaller for B (6.66 Å, 30°), A (6.80 Å, 90°) and E (9.98 Å, 30°). The comparison between B and C is of interest: B is further away from the paramagnetic center (smaller δ^{PC} contribution) but has a significantly larger isotropic shift; the

difference is likely a result of a larger δ^{FC} contribution. Similarly, E is very far away from the ytterbium; the δ^{PC} contribution is therefore small. Thus, since δ^{para} is large for B and E (and both have small δ^{PC} contributions) it means that E and B must have a significant δ^{FC} contribution. A is more problematic because both δ^{PC} and δ^{para} are small. It is thus difficult to draw conclusions concerning the magnitude of δ^{FC}. Likewise, although δ^{para} is large for D, the contributions are more difficult to disentangle, since both δ^{PC} and δ^{FC} could be sizeable for this resonance, and of similar values.

The presence of spin density on both the bipym and diketimine components of the Mabiq ligand, as deduced from the NMR data, indicates that both the SOMO and LUMO of the analogous monometallic [Ni(Mabiq$^{\bullet}$)] (Figure S5) might be populated in a mixed configuration in **3** due to the coordination of the ytterbocene. Therefore, the overall spin density around the nickel center is significantly modified compared to that of the monometallic [Ni(Mabiq$^{\bullet}$)] (Figure S5).[44] As such, several descriptions of the ground state electronic structure of **3** can be considered. Studies on the related $(Cp^*)_2Yb(bipym)NiMe_2$ complex highlighted the complexity in assigning electronic structures of systems containing lanthanides, transition metal ions and redox-active ligands.[42] Variable-temperature (VT) NMR and magnetic susceptibility data provided useful insight in this regard. Since both δ^{PC} and δ^{FC} are inversely dependent on temperature, we plotted the various ^{1}H-NMR resonances versus 1/T (Figures S6-S9; representative example given in Figure 5). The VT-NMR plots support our assignments of the resonances in **3** as determined from the room temperature spectrum. The protons associated with significant spin density display the largest temperature dependence (D, E and B), while the curvature indicates a deviation from Curie behavior. Similar deviation from Curie behavior was also observed in the $(Cp^*)_2Yb(bipym)NiMe_2$ system — and in other similar compounds — for

the resonances most shifted by the paramagnetic center.[41, 42, 53] The magnetic behavior of **3** is likely a result of magnetic exchange coupling between the single electrons on the Yb and Ni-Mabiq fragments. To test this hypothesis and further assess the electronic structure of **3**, solid-state magnetic susceptibility data were obtained.

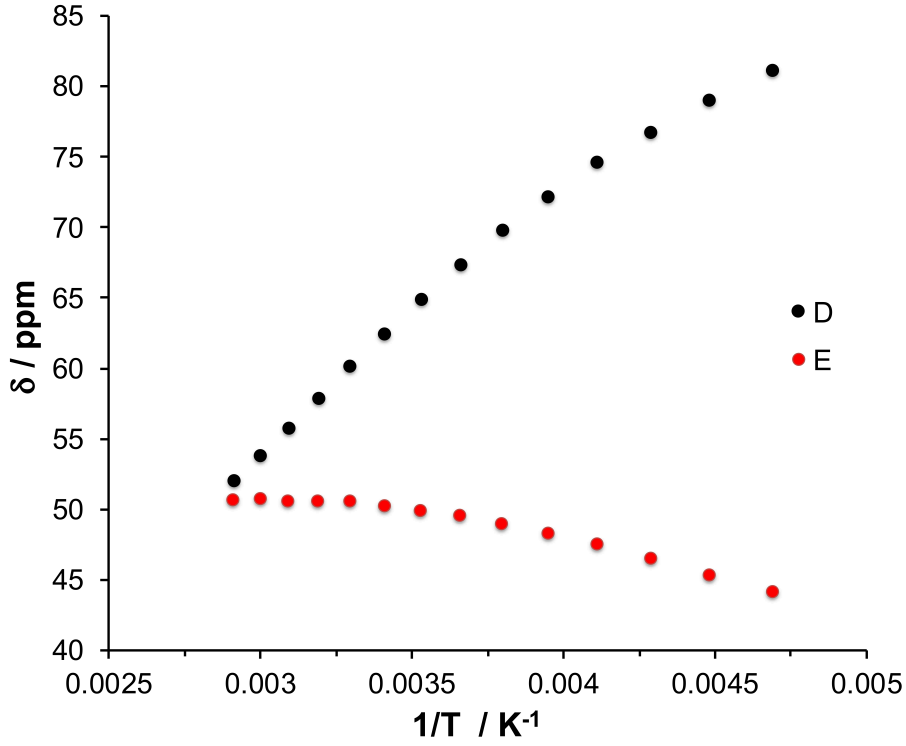

Figure 5. Variable temperature ^{1}H-NMR chemical shifts (δ) versus 1/T of the most strongly shifted protons assigned D and E in the ^{1}H-NMR spectrum of **3** (Figure 4).

The χT and 1/χ versus T plots derived from the magnetic susceptibility data are depicted in Figure 6. χT is 1.91 cm^3 K mol^{-1} at 300 K, and declines gradually with decreasing temperature, reaching values of 0.7 and 0.5 cm^3 K mol^{-1} at 10 and 2 K, respectively. In lanthanide compounds, the spin-orbit coupling is large and thus, the $^{2}F_{7/2}$ state should be considered for an Yb(III). Note that the theoretical value is then 2.54 emu mol^{-1} at room temperature, which decreases with

decreasing temperature because of the depopulation of the crystal field states.[54] The low temperature value for a $^2F_{7/2}$ is usually 1.2 – 2.0 emu mol^{-1}.

The electronic ground state structure can typically be inferred from the measurement of χT at 2 K. Previous investigations on bipyridine and phenanthroline adducts of Cp^*_2Yb showed that the presence of a redox-active ligand has a dramatic impact on the electronic structure and magnetic properties of the compound compared to those with a conventional innocent ligand.[53, 54] The Ln-bipyridine compound was characterized by a multiconfigurational singlet ground state and contained an intermediate-valent ytterbium (between +2 and +3). In contrast, the phenanthroline adducts have clear triplet ground states. By comparison with these related systems, we postulate that **3** has nearly degenerate singlet and triplet states, which contribute to the observed magnetism at low temperature. Indeed, on the one hand, the highest expected limiting value of χT is that of the triplet of 1.5 to 2.4 emu mol^{-1}, based on the value for a $^2F_{7/2}$ (Yb^{III}) ground state (usually 1.2 – 2.0 emu mol^{-1}) added to the typical 0.36 emu mol^{-1} value for a radical on a π system. On the other hand, the lowest limiting value is close to zero for a singlet (Van Vleck paramagnetism). However, in the case of **3** this value is low but not zero. Therefore, the data is neither in agreement with a clear singlet (S = 0) nor triplet (S = 1) ground state. Thus, the intermediate value of 0.5 emu mol^{-1} clearly indicates a situation in which the triplet and singlet are of very similar energy.

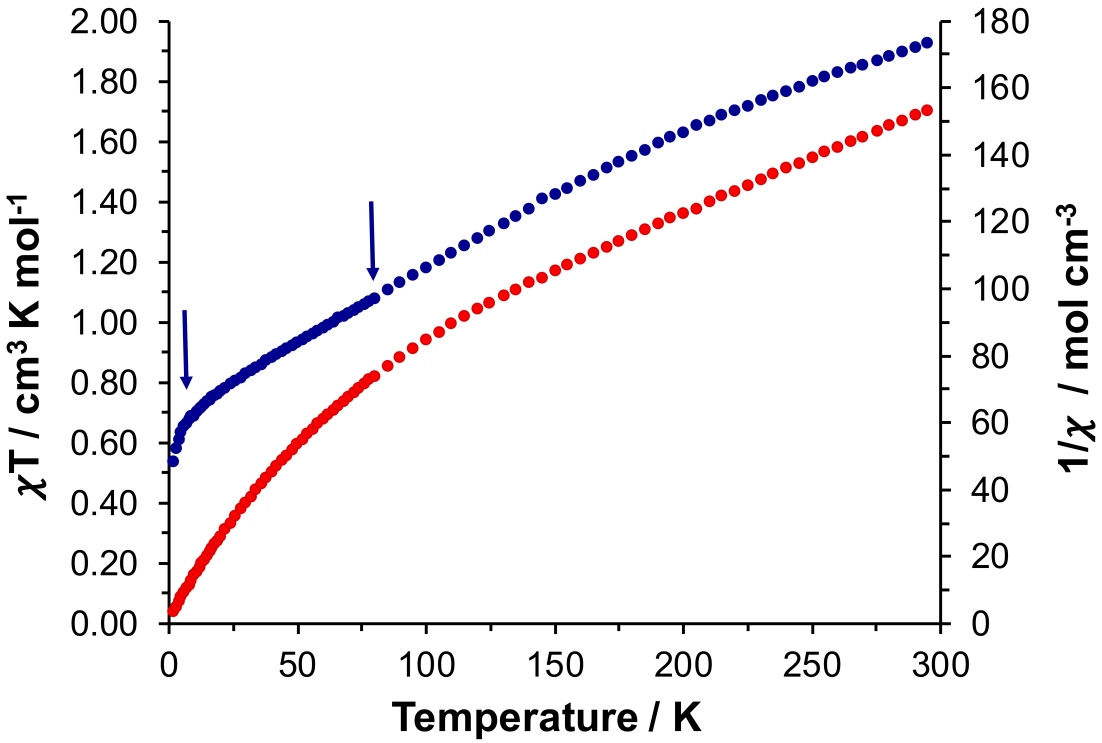

Figure 6. χT (blue) and 1/χ (red) plots as functions of temperature, T, for **3** measured at 0.5 T over the range 2 – 300 K. Inflection points in the χT plot are indicated by the arrows at ~10 and ~80 K.

The M vs H plot provides further evidence of a partially populated triplet state (Figure S10). The saturation of magnetism is typical for the $^2F_{7/2}$ state of the ytterbium, suggesting the population of a triplet state at low temperature. The evolution of the magnetic susceptibility with the temperature also is in agreement with the population of several energy states of different electronic nature and with a small difference in energy. The 1/χ vs T plot exhibits linear behavior from approximately 300 to 100 K, with a visible deviation from linearity at lower temperatures. The location of the curvature in the above plot corresponds with the inflection points around 10 and 80 K in the χT vs T plot. This non-linear behavior below 100 K also indicates population of

multiple states at the lower temperatures. Similar magnetic behavior has been observed in other systems with multiple intermediate-valent singlet states, and can be explained by the Boltzmann distribution between the states when the temperature changes.[41, 49, 53, 54] In the case of **3**, similar to the $Cp^*_2Yb(5,6\text{-}Me_2phenanthroline)$ complex, the inflection point is rather flat, which prevents any quantitative analysis of the data. Therefore, the data simply indicates that both intermediate-valent singlet states and the triplet state are very close in energy (Scheme S2). The necessary CASSCF computations that could rationalize this interpretation were attempted but were too large for the capabilities of our lab.[49, 55]

We note that the magnetic data for the Yb-Ni complex is in contrast to our previously reported dicobalt Mabiq complex, $Co_2(Mabiq)Cl_3$, which exhibited a negligible exchange coupling constant (J = 0.47 cm^{-1}), denoting weak communication between the two Co^{II} centers.[46] Coordination of a Cu^{I} ion to the outer Mabiq site also appeared to have a minimal influence on the electronic structure of the [Cu(Mabiq$^{\bullet}$)] site, based on the redox properties and results of DFT calculations for $[Cu_2(Mabiq)(PPh_3)_2(OTf)]$ compared with data for the monometallic complex.[47] In contrast, the combined magnetism and NMR spectroscopic data for **3** demonstrate that coordination of the ytterbocene to the Mabiq bipym site clearly leads to more significant coupling between the two units (formation of low-lying open-shell singlet(s)) and significantly modulates the extent of delocalization of the residual spin density.

CONCLUSIONS

In summary, we have synthesized and fully characterized a novel heterobimetallic Yb-Ni Mabiq complex, $[(Cp^*)_2Yb(Mabiq)Ni]BArF$. This represents the first mixed lanthanide/transition metal compound in the Mabiq family and a noteworthy addition to the class of 3d-4f compounds —

particularly those comprised of redox-active ligands. Our studies demonstrate that the peripheral Yb markedly influences the redox properties and electronic structure of the M-Mabiq site, which was not apparent in our homobimetallic transition metal Mabiq complexes. Consequently, the coordination of lanthanides offers a means to tune the reactivity, and potentially the photochemical properties, of the macrocyclic M-Mabiq unit. With respect to the latter, the combination of lanthanides with π-conjugated molecules and d-block ions offers a strategy for luminescence sensitization; select lanthanides also have recently been explored for photoredox catalytic applications.[56, 57] With regard to magnetic properties, the effect of other lanthanides in the outer Mabiq position — e.g. Dy^{III}, which has shown particular promise for SMMs — is of interest, since these metal ions may exhibit enhanced exchange interactions.[58] A positive influence of diamagnetic 3d ions, particularly Zn^{II}, on SMM behavior also was demonstrated.[59-61] M···M exchange interactions and magnetic properties of the bimetallic Mabiq complexes clearly are dependent on the nature of the metal centers. Therefore, varied combinations of 3d and 4f ions in the Mabiq system, offer significant opportunities for fine-tuning the Mabiq systems for applications in catalysis, photochemistry and magnetism.

EXPERIMENTAL SECTION

General Procedures. Chemicals not synthesized directly in lab were purchased from commercial sources and were used without further purification unless otherwise noted. Toluene and THF were refluxed and distilled over sodium with benzophenone as an indicator and stored over activated molecular sieves (4 Å) under argon. All other solvents were dried using a solvent purification system (MBSPS 800; MBraun), deoxygenated via freeze-pump-thaw procedure and stored over molecular sieves (3 or 4 Å) under argon. H(Mabiq) was synthesized as previously described.[43] NaBArF was synthesized as previously described (82% yield; Anal. Calcd for $C_{33}H_{12}BF_{24}Na$: C, 43,34; H, 1.36. Found C, 43.08, H, 1.33%).[62] Metal complexes were synthesized under inert atmosphere (Ar) using standard Schlenk and glovebox techniques.

Synthesis of [Ni(Mabiq)]BArF (2). NaBArF (251 mg, 283 μmol) was dissolved in MeCN (12 mL) and added dropwise to a stirred solution of [Ni(Mabiq)]Cl (180 mg, 283 μmol) in MeCN (26 mL). The solution was stirred at room temperature for 1 h and filtered. The solvent was removed under vacuum and the crude solid dissolved in Et_2O. The product was recrystallized by slow diffusion of the solution into hexane to yield dark yellow crystals suitable for single-crystal XRD (162 mg, 39%).

^{1}H-NMR ($CDCl_3$, 400 MHz, 300 K) δ, ppm: 9.17 (dd, J = 8.4, 1.4 Hz, 2H), 8.55 (m, 2H), 8.27 (ddd, J = 8.5, 7.0, 1.4 Hz, 2H) 8.00 (ddd, J = 8.2, 7.1, 1.1 Hz, 2H), 7.67 (s, 8H), 7.48 (s, 4H), 6.57 (s, 1H), 1.40 (s, 12H), 1.34 (s, 12H). ^{11}B-NMR ($CDCl_3$, 400 MHz, 300 K) δ, ppm: -6.60 (s). Anal. Calcd for $C_{65}H_{45}N_8BF_{24}Ni$: C, 53.34; H, 3.10; N, 7.66. Found: C, 53.17; H, 3.04; N, 7.70%. UV-vis [λ_{max}, nm (ε, M^{-1} cm^{-1}), THF]: 456 (1.8×10^4), 316 (4.0×10^4).

Synthesis of [(Cp*)$_2$Yb(Mabiq)Ni]BArF (3). (Cp*)$_2$YbOEt$_2$ (28.30 mg, 54.66 μmol) in cold THF (-35 °C, 0.4 mL) was added dropwise with stirring to [Ni(Mabiq)]BArF (79.90 mg, 54.66

μmol) in cold THF (1.6 mL). The solution was stirred at room temperature for 24 h, filtered over celite and the solvent removed under vacuum. The crude compound was recrystallized by slow diffusion of octane into a solution of toluene to yield brown crystals suitable for single-crystal XRD. Additional product could be isolated by layering octane onto the filtrate (81 mg, 78 %). ^{1}H-NMR (C_6D_6, 400 MHz, 300 K) δ, ppm: 63.54 (s, 2H), 46.33 (s, 1H), 14.53 (s, 2H), 7.58 (s, 8H), 6.73 (s, 4H), 3.64 (s, 12H), 2.07 (s, 12H), 0.96 (s, 2H), -0.76 (s, 30H), -4.65 (s, 2H). ^{11}B-NMR (C_6D_6, 400 MHz, 300 K) δ, ppm: -6.57 (s). Anal. Calcd for $C_{85}H_{75}BF_{24}N_8NiYb$: C, 53.53; H, 3.96; N, 5.88. Found: C, 53.53; H, 4.32; N, 5.51%. UV-vis [λ_{max}, nm (ε, M^{-1} cm^{-1}), THF]: 794 (2.9×10^3), 708 (1.8×10^3), 451 (1.9×10^4), 431 (1.9×10^4), 317 (4.3×10^4).

Physical Measurements. NMR measurements were performed with a Bruker Avance Ultrashield (400 MHz) spectrometer and analyzed using MestReNova (v12.0.4). Variable temperature NMR measurements were performed with a Bruker Avance III NMR spectrometer. Chemical shifts are reported in parts per million (ppm, scale) relative to the signal of the relevant deuterated solvent ($CDCl_3$ δ = 7.26 ppm; C_6D_6 δ = 7.16 ppm; THF-d_8 δ = 3.58, 1.73 ppm; acetone-d_6 δ = 2.05 ppm). Coupling constants (J) are given in hertz (Hz) and reported with multiplicity (s = singlet, d = doublet, t = triplet, q = quartet, m = multiplet). Electronic spectra were measured on an Agilent Cary 60 UV-vis spectrophotometer. Microanalyses were carried out at the Technische Universität München. Electrochemical measurements were carried out using an Emstat 3+ PalmSense potentiostat using a three-electrode cell equipped with glassy carbon working and counter electrodes and $Ag/AgNO_3$ reference electrode. Samples were measured (0.1-0.2 V s^{-1}; 0.1 M $[N(n\text{-}Bu)_4]PF_6$; in THF) under inert conditions and potentials are reported with reference to an internal standard of ferrocenium/ferrocene ($Fc^{+/0}$). Magnetic

susceptibility measurements for **3** were made. on powder in sealed quartz tubes on a Quantum Design SQUID at 0.5 and 2 T.

Crystallography. The crystallographic data was collected on a X-ray single crystal diffractometer, equipped with a CMOS detector (Bruker APEX III, κ-CMOS), a rotating anode (Bruker AXS, FR591) with Mo Kα radiation (λ = 0.71073 Å) and a MONTEL mirror optic by using the APEX3 software package or equipped with a CCD detector (Bruker APEX II, κ-CCD), a fine-focus sealed tube and a Triumph monochromator using the APEX2 software package.[63] The crystal was picked from perfluorinated ether and fixed on top of a Mitegen® microsampler and transferred to the diffractometer. The measurement was carried out under a constant stream of cold nitrogen. A matrix scan was used to determine the initial unit cell parameters. SAINT, as implemented in the APEX3 suite, was used to merge and correct the reflections for Lorenz and polarization effects, scan speed, and background.[64] Absorption corrections containing odd and even ordered spherical harmonics were performed using SADABS.[65] Space group assignments were established using systematic absences, E statistics, and successful refinement of the structures. Structures were solved using the intrinsic phasing method (SHELXT), which also supported the correct assignment of the space groups, and were refined against all data using SHELXLE in conjunction with SHELXL-2014 or Olex2.[66-69] Hydrogen atoms were calculated to the ideal position and refined employing a riding model with isotropic thermal parameters. Non-hydrogen atoms were refined with anisotropic displacement parameters. The images of the crystal structure were generated using Mercury.[70] We observed for structure **3** several non-merohedral twinning (as observed by non-indexable Bragg reflexes) in all of the tested single crystal samples, which we were not able to resolve better in the represented model.

ASSOCIATED CONTENT

Supporting Information

The Supporting Information is available free of charge on the [website] at DOI: [doi] (hyperlink PDF)

Accession Codes

CCDC 2036911–2036913 contain the supplementary crystallographic data for this paper. These data can be obtained free of charge via www.ccdc.cam.ac.uk/data_request/cif, or by emailing data_request@ccdc.cam.ac.uk, or by contacting The Cambridge Crystallographic Data Centre, 12 Union Road, Cambridge CB12 1EZ, UK; fax: +44 1223 336033.

AUTHOR INFORMATION

Corresponding Authors

*E-mail: corinna.hess@ch.tum.de

*E-mail: gregory.nocton@polytechnique.edu

Author Contributions

The manuscript was written through contributions of all authors. All authors have given approval to the final version of the manuscript.

Funding Sources

This work is part of a project that has received funding from the *European Research Council (ERC)* under *European Union's Horizon 2020 research and innovation program* under grant agreement No 716314.

ACKNOWLEDGMENTS

We thank Dr. Alex Pöthig for contributions to the crystallography. SB gratefully acknowledges the TUM IGSSE, for funding. CNRS and École Polytechnique are thanked for funding.

REFERENCES

1. Costes, J. P.; Dahan, F.; Dupuis, A.; Laurent, J. P., A General Route to Strictly Dinuclear Cu(II)/Ln(III) Complexes. Structural Determination and Magnetic Behavior of Two Cu(II)/Gd(III) Complexes. *Inorg. Chem.* **1997,** *36* (16), 3429-3433.
2. Costisor, O.; Linert, W., On polynuclear complexes in 3d-4f system. *Rev. Inorg. Chem.* **2005,** *25* (1), 13-54.
3. Chen, F.-F.; Chen, Z.-Q.; Bian, Z.-Q.; Huang, C.-H., Sensitized luminescence from lanthanides in d–f bimetallic complexes. *Coord. Chem. Rev.* **2010,** *254* (9-10), 991-1010.
4. Chakraborty, A.; Acharya, J.; Chandrasekhar, V., Ferrocene-Supported Compartmental Ligands for the Assembly of 3d/4f Complexes. *ACS Omega* **2020,** *5* (16), 9046-9054.
5. Osa, S.; Kido, T.; Matsumoto, N.; Re, N.; Pochaba, A.; Mrozinski, J., A tetranuclear 3d− 4f single molecule magnet:$[Cu^{II}LTb^{III}(hfac)_2]_2$. *J. Am. Chem. Soc.* **2004,** *126* (2), 420-421.
6. Andruh, M.; Costes, J.-P.; Diaz, C.; Gao, S., 3d− 4f combined chemistry: synthetic strategies and magnetic properties. *Inorg. Chem.* **2009,** *48* (8), 3342-3359.
7. Rosado Piquer, L.; Sanudo, E. C., Heterometallic 3d-4f single-molecule magnets. *Dalton Trans.* **2015,** *44* (19), 8771-80.
8. Liu, K.; Shi, W.; Cheng, P., Toward heterometallic single-molecule magnets: Synthetic strategy, structures and properties of 3d–4f discrete complexes. *Coord. Chem. Rev.* **2015,** *289*, 74-122.
9. Dey, A.; Acharya, J.; Chandrasekhar, V., Heterometallic 3d–4f Complexes as Single-Molecule Magnets. *Chem. Asian J.* **2019,** *14* (24), 4433-4453.
10. Langley, S. K.; Wielechowski, D. P.; Vieru, V.; Chilton, N. F.; Moubaraki, B.; Abrahams, B. F.; Chibotaru, L. F.; Murray, K. S., A $\{Cr^{III}_2Dy^{III}_2\}$ Single-Molecule Magnet: Enhancing the Blocking Temperature through 3d Magnetic Exchange. *Angew. Chem. Int. Ed.* **2013,** *52* (46), 12014-12019.
11. Langley, S. K.; Le, C.; Ungur, L.; Moubaraki, B.; Abrahams, B. F.; Chibotaru, L. F.; Murray, K. S., Heterometallic 3d–4f Single-Molecule Magnets: Ligand and Metal Ion Influences on the Magnetic Relaxation. *Inorg. Chem.* **2015,** *54* (7), 3631-3642.
12. Rinehart, J. D.; Fang, M.; Evans, W. J.; Long, J. R., Strong exchange and magnetic blocking in N_2^{3-}-radical-bridged lanthanide complexes. *Nat. Chem.* **2011,** *3* (7), 538-542.
13. Moreno Pineda, E.; Chilton, N. F.; Tuna, F.; Winpenny, R. E.; McInnes, E. J., Systematic Study of a Family of Butterfly-Like $\{M_2Ln_2\}$ Molecular Magnets (M= Mg^{II}, Mn^{III}, Co^{II}, Ni^{II}, and Cu^{II}; Ln= Y^{III}, Gd^{III}, Tb^{III}, Dy^{III}, Ho^{III}, and Er^{III}). *Inorg. Chem.* **2015,** *54* (12), 5930-5941.
14. Griffiths, K.; Kostakis, G. E., Transformative 3d–4f coordination cluster carriers. *Dalton Trans.* **2018,** *47* (35), 12011-12034.

15. Kumar, P.; Griffiths, K.; Anson, C. E.; Powell, A. K.; Kostakis, G. E., A tetranuclear $Cu^{II}_2Dy^{III}_2$ coordination cluster as a Suzuki (C–C) coupling reaction promoter. *Dalton Trans.* **2018,** *47* (48), 17202-17205.
16. Wang, L.; Xu, C.; Han, Q.; Tang, X.; Zhou, P.; Zhang, R.; Gao, G.; Xu, B.; Qin, W.; Liu, W., Ambient chemical fixation of CO_2 using a highly efficient heterometallic helicate catalyst system. *Chem. Commun.* **2018,** *54* (18), 2212-2215.
17. Gao, G.; Wang, L.; Zhang, R.; Xu, C.; Yang, H.; Liu, W., Hexanuclear 3d–4f complexes as efficient catalysts for converting CO_2 into cyclic carbonates. *Dalton Trans.* **2019,** *48* (12), 3941-3945.
18. Qu, L.; del Rosal, I.; Li, Q.; Wang, Y.; Yuan, D.; Yao, Y.; Maron, L., Efficient CO_2 transformation under ambient condition by heterobimetallic rare earth complexes: Experimental and computational evidences of a synergistic effect. *J. CO2 Util.* **2019,** *33*, 413-418.
19. Yang, H.; Gao, G.; Chen, W.; Wang, L.; Liu, W., Self-assembly of tetranuclear 3d–4f helicates as highly efficient catalysts for CO_2 cycloaddition reactions under mild conditions. *Dalton Trans.* **2020,** *49* (29), 10270-10277.
20. Ramirez, B. L.; Sharma, P.; Eisenhart, R. J.; Gagliardi, L.; Lu, C. C., Bimetallic nickel-lutetium complexes: tuning the properties and catalytic hydrogenation activity of the Ni site by varying the Lu coordination environment. *Chem. Sci.* **2019,** *10* (11), 3375-3384.
21. Lin, P.-H.; Takase, M. K.; Agapie, T., Investigations of the effect of the non-manganese metal in heterometallic-oxido cluster models of the oxygen evolving complex of photosystem II: lanthanides as substitutes for calcium. *Inorg. Chem.* **2015,** *54* (1), 59-64.
22. Lionetti, D.; Suseno, S.; Tsui, E. Y.; Lu, L.; Stich, T. A.; Carsch, K. M.; Nielsen, R. J.; Goddard, W. A.; Britt, R. D.; Agapie, T., Effects of Lewis Acidic Metal Ions (M) on Oxygen-Atom Transfer Reactivity of Heterometallic Mn_3MO_4 Cubane and $Fe_3MO(OH)$ and $Mn_3MO(OH)$ Clusters. *Inorg. Chem.* **2019,** *58* (4), 2336-2345.
23. Evangelisti, F.; Moré, R.; Hodel, F.; Luber, S.; Patzke, G. R., 3d–4f $\{Co^{II}_3Ln(OR)_4\}$ Cubanes as Bio-Inspired Water Oxidation Catalysts. *J. Am. Chem. Soc.* **2015,** *137* (34), 11076-11084.
24. Woodruff, D. N.; Winpenny, R. E.; Layfield, R. A., Lanthanide single-molecule magnets. *Chem. Rev.* **2013,** *113* (7), 5110-48.
25. Demir, S.; Jeon, I.-R.; Long, J. R.; Harris, T. D., Radical ligand-containing single-molecule magnets. *Coord. Chem. Rev.* **2015,** *289*, 149-176.
26. Chen, C.; Hu, Z.-B.; Ruan, H.; Zhao, Y.; Zhang, Y.-Q.; Tan, G.; Song, Y.; Wang, X., Tuning the Single-Molecule Magnetism of Dysprosium Complexes by a Redox-Noninnocent Diborane Ligand. *Organometallics* **2020**.
27. Lyaskovskyy, V.; de Bruin, B., Redox Non-Innocent Ligands: Versatile New Tools to Control Catalytic Reactions. *ACS Catal.* **2012,** *2* (2), 270-279.
28. Luca, O. R.; Crabtree, R. H., Redox-active ligands in catalysis. *Chem. Soc. Rev.* **2013,** *42* (4), 1440-1459.
29. Das, A.; Ren, Y.; Hessin, C.; Desage-El Murr, M., Copper catalysis with redox-active ligands. *Beilstein J. Org. Chem.* **2020,** *16* (1), 858-870.
30. Chirik, P. J.; Wieghardt, K., Radical ligands confer nobility on base-metal catalysts. *Science* **2010,** *327* (5967), 794-795.
31. Chirik, P. J., Preface: forum on redox-active ligands. *Inorg. Chem.* **2011,** *50* (20), 9737-9740.
32. Kaim, W., The Shrinking World of Innocent Ligands: Conventionaland Non-Conventional Redox-Active Ligands. *Eur. J. Inorg. Chem.* **2012,** *2012* (3), 343-348.

33. Buchwald, S. L.; Milstein, D., *Ligand Design in Metal Chemistry: Reactivity and Catalysis*. John Wiley & Sons: 2016.
34. Camp, C.; Guidal, V.; Biswas, B.; Pécaut, J.; Dubois, L.; Mazzanti, M., Multielectron redox chemistry of lanthanide Schiff-base complexes. *Chem. Sci.* **2012,** *3* (8), 2433-2448.
35. Andrez, J.; Bozoklu, G.; Nocton, G.; Pecaut, J.; Scopelliti, R.; Dubois, L.; Mazzanti, M., Lanthanide(II) Complexes Supported by N,O-Donor Tripodal Ligands: Synthesis, Structure, and Ligand-Dependent Redox Behavior. *Chem. Eur. J* **2015,** *21* (43), 15188-200.
36. Fedushkin, I. L.; Yambulatov, D. S.; Skatova, A. A.; Baranov, E. V.; Demeshko, S.; Bogomyakov, A. S.; Ovcharenko, V. I.; Zueva, E. M., Ytterbium and Europium Complexes of Redox-Active Ligands: Searching for Redox Isomerism. *Inorg. Chem.* **2017,** *56* (16), 9825-9833.
37. Hickson, J. R.; Horsewill, S. J.; Bamforth, C.; McGuire, J.; Wilson, C.; Sproules, S.; Farnaby, J. H., The modular synthesis of rare earth-transition metal heterobimetallic complexes utilizing a redox-active ligand. *Dalton Trans.* **2018,** *47* (31), 10692-10701.
38. Hickson, J. R.; Horsewill, S. J.; McGuire, J.; Wilson, C.; Sproules, S.; Farnaby, J. H., The semiquinone radical anion of 1,10-phenanthroline-5,6-dione: synthesis and rare earth coordination chemistry. *Chem. Commun.* **2018,** *54* (80), 11284-11287.
39. Jaoul, A.; Tricoire, M.; Moutet, J.; Cordier, M.; Clavaguera, C.; Nocton, G., Reversible electron transfer in organolanthanide chemistry. *Chem Sq* **2019,** *3*, 1.
40. McGuire, J.; Wilson, B.; McAllister, J.; Miras, H. N.; Wilson, C.; Sproules, S.; Farnaby, J. H., Molecular and electronic structure of the dithiooxalato radical ligand stabilised by rare earth coordination. *Dalton Trans.* **2019,** *48* (17), 5491-5495.
41. Goudy, V.; Jaoul, A.; Cordier, M.; Clavaguera, C.; Nocton, G., Tuning the Stability of Pd(IV) Intermediates Using a Redox Non-innocent Ligand Combined with an Organolanthanide Fragment. *J. Am. Chem. Soc.* **2017,** *139* (31), 10633-10636.
42. Wang, D.; Moutet, J.; Tricoire, M.; Cordier, M.; Nocton, G., Reactive Heterobimetallic Complex Combining Divalent Ytterbium and Dimethyl Nickel Fragments. *Inorganics* **2019,** *7* (5), 58.
43. Banerjee, P.; Company, A.; Weyhermüller, T.; Bill, E.; Hess, C. R., Zn and Fe Complexes Containing a Redox Active Macrocyclic Biquinazoline Ligand. *Inorg. Chem.* **2009,** *48* (7), 2944-2955.
44. Grubel, M.; Bosque, I.; Altmann, P. J.; Bach, T.; Hess, C. R., Redox and photocatalytic properties of a Ni(II) complex with a macrocyclic biquinazoline (Mabiq) ligand. *Chem. Sci.* **2018,** *9* (13), 3313-3317.
45. Kaspar, M.; Altmann, P. J.; Pothig, A.; Sproules, S.; Hess, C. R., A macrocyclic 'Co(0)' complex: the relevance of ligand non-innocence to reactivity. *Chem. Commun.* **2017,** *53* (53), 7282-7285.
46. Puttock, E. V.; Banerjee, P.; Kaspar, M.; Drennen, L.; Yufit, D. S.; Bill, E.; Sproules, S.; Hess, C. R., A Series of $[Co(Mabiq)Cl_{2-n}]$ (n = 0, 1, 2) Compounds and Evidence for the Elusive Bimetallic Form. *Inorg. Chem.* **2015,** *54* (12), 5864-73.
47. Stark, H. S.; Altmann, P. J.; Sproules, S.; Hess, C. R., Structural Characterization and Photochemical Properties of Mono- and Bimetallic Cu-Mabiq Complexes. *Inorg. Chem.* **2018,** *57* (11), 6401-6409.
48. Nocton, G.; Booth, C. H.; Maron, L.; Ricard, L.; Andersen, R. A., Carbon–Hydrogen Bond Breaking and Making in the Open-Shell Singlet Molecule Cp^*_2Yb (4,7-Me_2phen). *Organometallics* **2014,** *33* (23), 6819-6829.

49. Nocton, G.; Booth, C. H.; Maron, L.; Andersen, R. A., Thermal dihydrogen elimination from Cp^*_2Yb (4,5-diazafluorene). *Organometallics* **2013,** *32* (5), 1150-1158.
50. Veauthier, J. M.; Schelter, E. J.; Carlson, C. N.; Scott, B. L.; Re, R. E. D.; Thompson, J.; Kiplinger, J. L.; Morris, D. E.; John, K. D., Direct comparison of the magnetic and electronic properties of samarocene and ytterbocene terpyridine complexes. *Inorg. Chem.* **2008,** *47* (13), 5841-5849.
51. La Mar, G. N.; Horrocks, W. D.; Holm, R. H., *NMR of paramagnetic molecules: principles and applications*. Elsevier: 2016.
52. Lonnon, D. G.; Ball, G. E.; Taylor, I.; Craig, D. C.; Colbran, S. B., Fluxionality in a Paramagnetic Seven-Coordinate Iron(II) Complex: A Variable-Temperature, Two-Dimensional NMR and DFT Study. *Inorg. Chem.* **2009,** *48* (11), 4863-4872.
53. Booth, C. H.; Kazhdan, D.; Werkema, E. L.; Walter, M. D.; Lukens, W. W.; Bauer, E. D.; Hu, Y.-J.; Maron, L.; Eisenstein, O.; Head-Gordon, M.; Andersen, R. A., Intermediate-Valence Tautomerism in Decamethylytterbocene Complexes of Methyl-Substituted Bipyridines. *J. Am. Chem. Soc.* **2010,** *132* (49), 17537-17549.
54. Nocton, G.; Lukens, W. W.; Booth, C. H.; Rozenel, S. S.; Medling, S. A.; Maron, L.; Andersen, R. A., Reversible sigma C–C bond formation between phenanthroline ligands activated by $(C_5Me_5)_2Yb$. *J. Am. Chem. Soc.* **2014,** *136* (24), 8626-8641.
55. Booth, C. H.; Walter, M. D.; Kazhdan, D.; Hu, Y.-J.; Lukens, W. W.; Bauer, E. D.; Maron, L.; Eisenstein, O.; Andersen, R. A., Decamethylytterbocene complexes of bipyridines and diazabutadienes: Multiconfigurational ground states and open-shell singlet formation. *J. Am. Chem. Soc.* **2009,** *131* (18), 6480-6491.
56. Lo, W.-K.; Wong, W.-K.; Wong, W.-Y.; Guo, J.; Yeung, K.-T.; Cheng, Y.-K.; Yang, X.; Jones, R. A., Heterobimetallic Zn(II)−Ln(III) phenylene-bridged Schiff base complexes, computational studies, and evidence for singlet energy transfer as the main pathway in the sensitization of near-infrared Nd^{3+} luminescence. *Inorg. Chem.* **2006,** *45* (23), 9315-9325.
57. Meyer, A. U.; Slanina, T.; Heckel, A.; König, B., Lanthanide ions coupled with photoinduced electron transfer generate strong reduction potentials from visible light. *Chem. Eur. J* **2017,** *23* (33), 7900-7904.
58. Guo, F.-S.; Day, B. M.; Chen, Y.-C.; Tong, M.-L.; Mansikkamäki, A.; Layfield, R. A., Magnetic hysteresis up to 80 kelvin in a dysprosium metallocene single-molecule magnet. *Science* **2018,** *362* (6421), 1400-1403.
59. Upadhyay, A.; Singh, S. K.; Das, C.; Mondol, R.; Langley, S. K.; Murray, K. S.; Rajaraman, G.; Shanmugam, M., Enhancing the effective energy barrier of a Dy(III) SMM using a bridged diamagnetic Zn(II)ion. *Chem. Commun.* **2014,** *50* (64), 8838-8841.
60. Upadhyay, A.; Das, C.; Vaidya, S.; Singh, S. K.; Gupta, T.; Mondol, R.; Langley, S. K.; Murray, K. S.; Rajaraman, G.; Shanmugam, M., Role of the Diamagnetic Zinc(II) Ion in Determining the Electronic Structure of Lanthanide Single-Ion Magnets. *Chem. Eur. J.* **2017,** *23* (20), 4903-4916.
61. Costes, J. P.; Titos-Padilla, S.; Oyarzabal, I.; Gupta, T.; Duhayon, C.; Rajaraman, G.; Colacio, E., Effect of ligand substitution around the Dy^{III} on the SMM properties of dual-luminescent Zn–Dy and Zn–Dy–Zn complexes with large anisotropy energy barriers: a combined theoretical and experimental magnetostructural study. *Inorg. Chem.* **2016,** *55* (9), 4428-4440.

62. Yakelis, N. A.; Bergman, R. G., Safe preparation and purification of sodium tetrakis [(3,5-trifluoromethyl) phenyl] borate ($NaBArF_{24}$): reliable and sensitive analysis of water in solutions of fluorinated tetraarylborates. *Organometallics* **2005,** *24* (14), 3579-3581.
63. APEX Suite of Crystallographic Software, APEX 3, Version 2015-5. Bruker AXS Inc.: Madison, Wisconsin, USA 2015.
64. SAINT, Version 8.37A. Bruker AXS Inc.: Madison, Wisconsin, USA 2014; SAINT, Version 7.68A, Bruker AXS Inc.: Madison, Wisconsin, USA 2014.
65. SADABS, Version 2016/2. Bruker AXS Inc.: Madison, Wisconsin, USA 2014; SADABS, Version 2008/1. Bruker AXS Inc.: Madison, Wisconsin, USA 2014.
66. Sheldrick, G. M., SHELXT–Integrated space-group and crystal-structure determination. *Acta Crystallogr. A* **2015,** *71* (1), 3-8.
67. Sheldrick, G. M., Crystal structure refinement with SHELXL. *Acta Crystallogr. C* **2015,** *71* (1), 3-8.
68. Hübschle, C. B.; Sheldrick, G. M.; Dittrich, B., ShelXle: a Qt graphical user interface for SHELXL. *J. Appl. Crystallogr.* **2011,** *44* (6), 1281-1284.
69. Dolomanov, O. V.; Bourhis, L. J.; Gildea, R. J.; Howard, J. A.; Puschmann, H., OLEX2: a complete structure solution, refinement and analysis program. *J. Appl. Crystallogr.* **2009,** *42* (2), 339-341.
70. Macrae, C. F.; Bruno, I. J.; Chisholm, J. A.; Edgington, P. R.; McCabe, P.; Pidcock, E.; Rodriguez-Monge, L.; Taylor, R.; Streek, J.; Wood, P. A., Mercury CSD 2.0–new features for the visualization and investigation of crystal structures. *J. Appl. Crystallogr.* **2008,** *41* (2), 466-470.